Potential of mean force analysis of short boron nitride and carbon nanotubes insertion into cell membranes

A.A. Tsukanov[1]* and S.G. Psakhie[2,3]

[1] Skolkovo Institute of Science and Technologies, Moscow, 143026 Russia
[2] Institute of Strength Physics and Materials Science, Siberian Branch, Russian Academy of Sciences, Tomsk, 634055 Russia
[3] Tomsk Polytechnic University, Tomsk, 634050 Russia

Tubular nanostructures made of boron nitride are of great interest for nanomedicine. In particular, single-walled boron nitride nanotubes (BNNT) are considered as intracellular nanovectors that have good biocompatibility and potentially lower cytotoxicity than carbon nanoparticles. However, the nanoscale mechanisms of BNNT interaction with the cell membrane remain largely unknown. In this paper a short steered molecular dynamics study of BNNT insertion into a lipid bilayer is presented and its results are compared with the available free energy estimations for carbon nanotube (CNT) penetration. Two BNNT models having different sets of partial atomic charges (PAC) were utilized. Using potential of mean force analysis, the free energy profiles of CNT and two cases of BNNT were compared. The results show that a BNNT with partial charges of ±0.4 e has a similar free energy profile to CNT, but the depth of the free energy well is about 30% smaller than for CNT. Furthermore in contrast to membrane penetration by CNT, BNNT remains filled with water even when it is inside the lipid interior. In the second case, BNNT with PAC of ±1.05 e demonstrates hydrophilic behavior of the nanotube, and its penetration into the cell membrane is quite complicated. Moreover, in this case BNNT has a quasi-stable state on the lipid-water interface. The results suggest that BNNT is less cytotoxic than pristine CNT, however, further steered molecular dynamics investigations with lower pulling velocities and environmentally dependent PAC are necessary.

Keywords: boron nitride nanotube, cell membrane, cytotoxicity, free energy, steered molecular dynamics, potential of mean force

1. Introduction

Nanomedicine is a quickly developing research field at the intersection of biomedicine, chemistry and nanotechnology. Ever since carbon fullerenes (in 1985) [1] and nanotubes (NT) [2] were discovered (1991), they have been considered for biomedical applications [3–6]. This attention is mostly due to the unique physical properties and geometrical structure of these nanomaterials. Besides carbon, several compounds are known to form tubular nanostructures and fullerene-like hollow nanoparticles, i.e. aluminosilicate nanotubes (imogolite), which were synthesized in 1977 [7, 8], nanotubes based on layered tungsten disulfide, which were obtained in 1992 [9], fullerene-like nanostructures and nanotubes of other transition metal disulfides (MoS_2, WS_2, TiS_2, ZrS_2, NbS_2) [10, 11], boron nitride (BN) nanotubes, which were predicted in 1994 [12] and synthesized in 1995 [13], boron carbon nitride (BCN) nanotubes [14, 15], including BC_x and CN_x nanotubes [16], BN fullerene analogues (fulborenes) and fulborenites [17–19], aluminum oxide nanotubes and nanoballs [20], titanium dioxide nanotubes [21], vanadium oxide (V_2O_5) fullerene analogues [22], silicon nanotubes [23], and nanotubulenes of other inorganic compounds [24–26].

In the last decade boron nitride based nano-objects have been receiving increased attention. Boron nitride nanotubes in particular have potential applications in nanomedicine (see [27] and references therein). The crystal structure of BNNT is very similar to that of carbon nanotubes, where a hexagonal B_3N_3 cycle substitutes the aromatic carbon unit. Depending on chirality indexes BNNT, like CNT, might have “armchair”, “zigzag” or other intermediate structure. Nevertheless, BNNT and CNT possess different chemical and physical properties. Due to noticeable difference in electronegativity between boron and nitrogen atoms, BNNT has local electric dipole moments on its surface with positive charge on boron atoms and negative charge on nitrogen (naturally, the charges balance out so the net charge is zero). Such a charge distribution increases the interaction energy

* *Corresponding author*
Dr. Alexey A. Tsukanov, e-mail: a.a.tsukanov@yandex.ru

between the nanotube and a polar solvent, which tends to make the nanoparticles less hydrophobic. Moreover, in contrast to CNT, BNNTs demonstrate a direct and indirect piezoelectric effect [28]. This provides BNNT with the possibility to change its electric properties and to generate electric signals, which may be controlled, for example, by external ultrasonic waves [29]. Furthermore, despite the structural similarity with CNT, BNNT is chirality-independent dielectric material with a wide band gap [30]. Due to these and other properties, BNNT has been considered for many applications, including nanovectors for intercellular drug and gene delivery [31–33], nanosensors and nanotransducers [34], contrast agents in neutron capture anticancer therapy [35], tissue engineering [36], and as nanofillers for composite materials [37]. In addition, BNNT and CNT demonstrate different selectivity to ion types that may pass through the nanotube, and have therefore been suggested as artificial ion channels potentially useful for numerous biomedical applications [38]. Experimental investigations of BNNT with applications in nanomedicine are reviewed in [27]. An overview of theoretical studies, fabrication methods, physical properties, chemical functionalization and applications of BNNTs can be found in [39].

Unlike CNT, nanoscale mechanisms of BNNT's interaction with biomolecules, proteins, cell membranes are mostly unknown and poorly covered by computer simulations, including MD methods. To date, the only study that is touching on this bio-related direction is an investigation of the stability and insertion mechanism of BNNT into the lipid membrane, conducted by Thomas et al. using all-atom MD and SMD simulation [40]. The results obtained there indicate that (10, 0) armchair BNNT may spontaneously embed across the head group region of the lipids, which takes about 100 ns from the initial position of 1.5 nm above membrane surface. It was also found that BNNTs remain in the lipophilic zone of the model POPC bilayer during the extended simulation time (about 200 ns).

The main aim of the present study is to compare the free energy difference ΔF and the magnitude of free energy barrier F_{barr} of insertion of BNNT into a lipid bilayer with those for CNT insertion. Short nanotubes were chosen to avoid a multidimensionality of the problem, decreasing dependence on initial orientation of the penetrant.

2. Review of work on carbon nanotubes

In contrast to BNNT, the free energy of interaction between CNTs and lipid membranes was previously studied using MD. Baoukina et al. [41] conducted a broad study of the interaction of pristine and functionalized CNTs of different length, diameter, end termination and chemical modification with a DOPC lipid bilayer. This study used coarse-grained MD simulations based on the MARTINI force field [42–44]. Pristine CNTs and CNTs having hydrophilic groups with diameters in the range of 1.23–2.40 nm and lengths from 4.1 to 9.7 nm, both separately and within aggregates, were considered. In the framework of our study we are interested in the case of short thin non-functionalized CNT at the lower end of the range (diameter 1.23 nm, length 4.1 nm). The magnitude of the free energy barrier for such a CNT has an order of 1–10 kJ/mol, the maximum being at a distance of 3.5–4.5 nm from the bilayer center, depending of the orientation of the nanotube (for pristine CNT with length 6.5 nm Baoukina et al. [41] have obtained F_{barr} = 5–14 kJ/mol). The free energy minimum of about –300 kJ/mol is found near the membrane middle plane, and this value doesn't depend on the tube's orientation, due to the shortness of the penetrant.

Kraszewski et al. [45] considered non-functionalized CNT and CNTs with different number of amino-derivative ligands on the surface. In particular, the free energy profile for the insertion of pure capped (6, 6) single-walled CNT into a POPC lipid membrane was evaluated. The CNT model had 0.8 nm in diameter and a length of 5 nm. A free energy barrier of ~21 kJ/mol at the lipid/water interface and a local minimum of –88 kJ/mol at 0.3–0.5 nm from the membrane center were observed.

Höfinger et al. [46] evaluated environmental free energy landscapes for various orientations of single CNTs with different lengths and CNT bundles of different size. For this purpose, the membrane mimicry approach [47] was employed there. For short single CNT, 0.8 nm in diameter and 2.1 nm in length, the free energy barrier is about 15 kJ/mol and is located at ~2.9 nm from the bilayer center. The free energy minimum at 0.0–1.1 nm from the bilayer center has a depth $\Delta F \approx -170$ kJ/mol.

Gangupomu and Capaldi [48] used all-atom MD to compute forces and the change in free energy during the penetration of a single-walled carbon nanotube (SWNT) into a pure POPC lipid bilayer and a POPC/cholesterol membrane. The constant-velocity steered MD (cv-SMD) approach was applied to calculate potential mean force (PMF) profiles. At the lowest pulling velocity (v = 1 nm/ns) the free energy barrier of perforation of the upper lipid monolayer by a CNT having 1 nm in diameter and 2 nm in length was estimated at about 150 kJ. This large value may be explained by irreversible disruption of the membrane due to the relatively high velocity of the pulling process.

Pogodin and Baulin [49] estimated free energy change during insertion of CNTs into a lipid bilayer using the single chain mean field theory [50]. A range of CNT diameters from 1.00 to 4.86 nm, as well as different values of the interaction parameter ε_T between CNT and the hydrophobic core of the lipid bilayer were considered. Values from $\varepsilon_T = 0$ (steric repulsion) to $\varepsilon_T = -6.3\ k_{\text{B}}T$ (strong hydrophobicity) were used in the model. The free energy minimum for the case of highly hydrophobic thin CNTs having 1 nm in diameter was estimated at about –180 kJ/mol [49]. These results were obtained for perpendicularly constrained nanotubes of "infinite" length (more than the bilayer thickness).

Table 1. Comparison of estimates of free energy difference and barrier energy of intercalation of short and/or thin pristine (non-functionalized) CNTs in cell membranes obtained using numerical simulations

Study	D, nm	L, nm	ΔF, kJ/mol (kcal/mol)	Free energy minimum position, nm	F_{barr}, kJ/mol (kcal/mol)	Barrier maximum position, nm
[41]	**1.23**	**4.10**	–300 (–72)	≈0.0	~10 (2.5)	3.5–4.5
[45]	**0.80**	**5.00**	–88 (**–21**)	0.3–0.5	20.5 (**4.9**)	2.0–2.5
[46]	**0.80**	**2.10**	–167 (**–40**)	0.0–**1.1**	14.6 (**3.5**)	≈**2.9**
[48]	**1.00**	**2.00**	–	–	146 (**35**)	–
[49]	**1.00**	3.77*	–180 (**–72.1**k_BT)	1.255**	≈0	∞
(C_{60}) [51]	0.70	0.70	–92 (**–22**)	**0.6–0.7**	≈0	∞
This study CNT	0.68	1.11	–103 (–25)	0.7–0.8	3.3–6.3	2.5–2.6
This study BNNT Case 1, q ± 0.40 e	0.69	1.13	–72 (–17)	0.7–1.0	0–20	2.1–2.3
This study BNNT Case 2, q ± 1.05 e	0.69	1.13	–11 (–2.7)	2.4–2.6	105 (25)	≈0

* Length of inserted part of the nanotube.
** Center of mass position of the inserted part of the nanotube.
Bold font marks values that are explicitly reported in the respective study.

Table 2. Models parameters of the numerical studies in this review

Study	Chirality, open (O) / capped (C)	Model level	Base FF (if applicable) and carbon LJ parameters	Membrane model	T, K	Method
[41]	(CG), C	CG	MARTINI [42–44]	DOPC (648 pcs.)	310	US
[45]	(6, 6), C	AA/UA	CHARMM27-UA σ = 0.3895 nm [52] ε = 0.276 kJ/mol	POPC (180 pcs.) **0.649** nm^2 per lipid	300	ABF [53, 54]
[46]	(10, 0), C	AA/MMA	AMBER σ = 0.3400 nm ε = 0.360 kJ/mol	MMA [47]	–	
[48]	(–, –), O	AA	CHARMM σ = not shown ε = not shown	POPC (200 pcs.)	310	cv-SMD v = **1.00** nm/ns
[49]	Cylinder	SCMF/CG	SCMF $\varepsilon_T = -6.3k_BT$	DMPC	in k_BT (~301 K)	Minimization of the free energy functional
[51]	C_{60} fullerene	AA	CHARMM27 σ = 0.3895 nm [52] ε = 0.276 kJ/mol	DMPC (52 pcs.) **0.618** nm^2 per lipid	310	z-constrained MD
[@]/CNT	(5, 5), O	AA/UA [55]	CHARMM36-UA σ = 0.3534 nm [56] ε = 0.2929 kJ/mol	POPC (104 pcs.) **0.633** nm^2 per lipid	310	cv-SMD v = **0.05** nm/ns
[@]/$BNNT_1$	(5, 5), O	AA/UA	CHARMM36-UA	POPC (104 pcs.) **0.632** nm^2 per lipid	310	cv-SMD v = **0.05** nm/ns
[@]/$BNNT_2$	(5, 5), O	AA/UA	CHARMM36-UA	POPC (104 pcs.) **0.649** nm^2 per lipid	310	cv-SMD v = **0.05** nm/ns

[@]—means this study, AA—all-atom MD simulation, UA—united atom model (implicit hydrogen in acyl lipid chains), CG—coarse-grained MD simulation, FF—force field, MMA—membrane mimicry approach [47], cv-SMD—constant velocity steered MD, SCMF—single chain mean field theory [50]. LJ—Lennard-Jones parameters, US—umbrella sampling [57], ABF—adaptive biasing force method [53, 54].

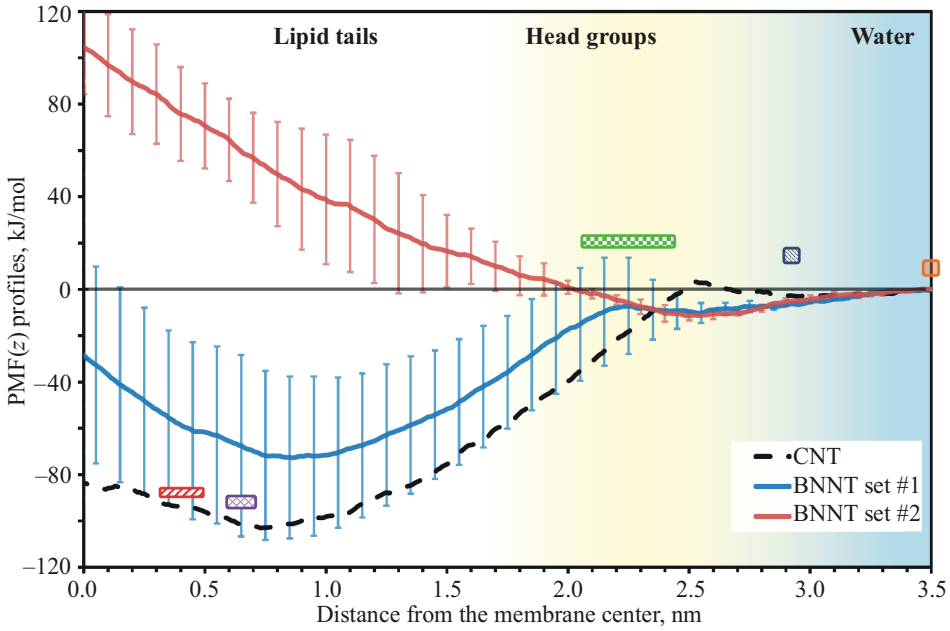

Fig. 1. PMF profiles versus distance of nanotube center of mass from bilayer center, cv-SMD result with v = 0.05 nm/ns. Blue curve—(5, 5) BNNT with partial charges ±0.4 e (set #1), red—BNNT with charges ±1.05 e (set #2), dashed black line—(5, 5) CNT. The red and green rectangles approximately show, respectively, the local free energy minimum and the free energy barrier from results of [45]. The purple rectangle is placed according to [51], the dark-blue square indicates the free energy barrier estimated in [46], the orange square roughly indicates the energy barrier from [41]. Background shading: blue—water, yellow—lipid head groups region, white—lipophilic zone.

Obviously, the free energy profile would be different for finite-length CNTs with rotational freedom. However, based on Pogodin and Baulin issues we could roughly define the position of the free energy minimum, assuming that the length of the inserted portion is a CNT length and that CNT position is the position of the center of mass of the inserted fragment. Thus, the position of F minimum would be 1.255 nm from the bilayer middle plane.

Summarizing the above review, we find that the free energy of penetration of short and thin carbon nanotubes into cell membranes has been estimated to be 88–300 kJ/mol in magnitude, depending on size and orientation of the penetrant (Table 1). The first free energy barrier varies from ~10 to 21 kJ/mol, however, "barrier-less" insertion (F_{barr} ~ 0) and large barriers of up to 150 kJ/mol have also been reported. The latter value corresponds to the energy required to perforate a lipid monolayer (single leaflet), most likely in an irreversible process [48], which is why we do not take this study into account. The results mentioned in [41, 45, 46, 48, 49] as well as our own results are presented in Table 1, the corresponding model parameters are summarized in Table 2.

In the present study, in addition to our primary objective, we simulated the translocation of a short (5, 5) carbon SWNT into a lipid bilayer. A single 80 ns long SMD simulation was performed. The results of PMF profile evaluation are presented in Fig. 1 as a dashed black line. (The blue and red curves correspond to two different sets of boron nitride NTs and will be discussed further in the next.) A rough estimate of the free energy minimum for (5, 5) CNT ΔF_{CNT}: –103 kJ/mol, reached 0.7–0.8 nm from the bilayer center (Fig. 1, black dashed curve). Due to the short length of the considered CNT, its behavior should be very similar to that of fullerenes C_{60}. If we compare our results with the results for C_{60} obtained by Bedrov et al. [51] (ΔF_{C60} = –92 kJ/mol, observed around 0.6–0.7 nm from the center), we find them in good agreement.

Note also, that according to an approximate rule from [45], the free energy barrier of pristine capped CNT translocation into a lipid bilayer can be roughly estimated as ~1 kcal/mol per 1 nm of length and per 1 nm in diameter, which in our case results in an estimation of F^*_{barr} ~ 1.11×0.68 kcal/mol ~ 3.2 kJ/mol, while in our simulation this value is F_{barr} ~ 3.3 kJ/mol from the initial free energy level or ~6.3 kJ/mol from the first local minimum observed at the position 2.9–3.0 nm (Fig. 1, black dashed curve).

Thus, our estimation of the free energy profile for CNT does not contradict any published data for similar conditions. The obtained value of ΔF is in good agreement with results of [45, 51], the obtained magnitude of the barrier F_{barr} is in between the results of [49, 51] and [41, 46] (see Fig. 1). In the following, we will use the evaluated PMF profile for CNT as a control line to compare the BNNT results with.

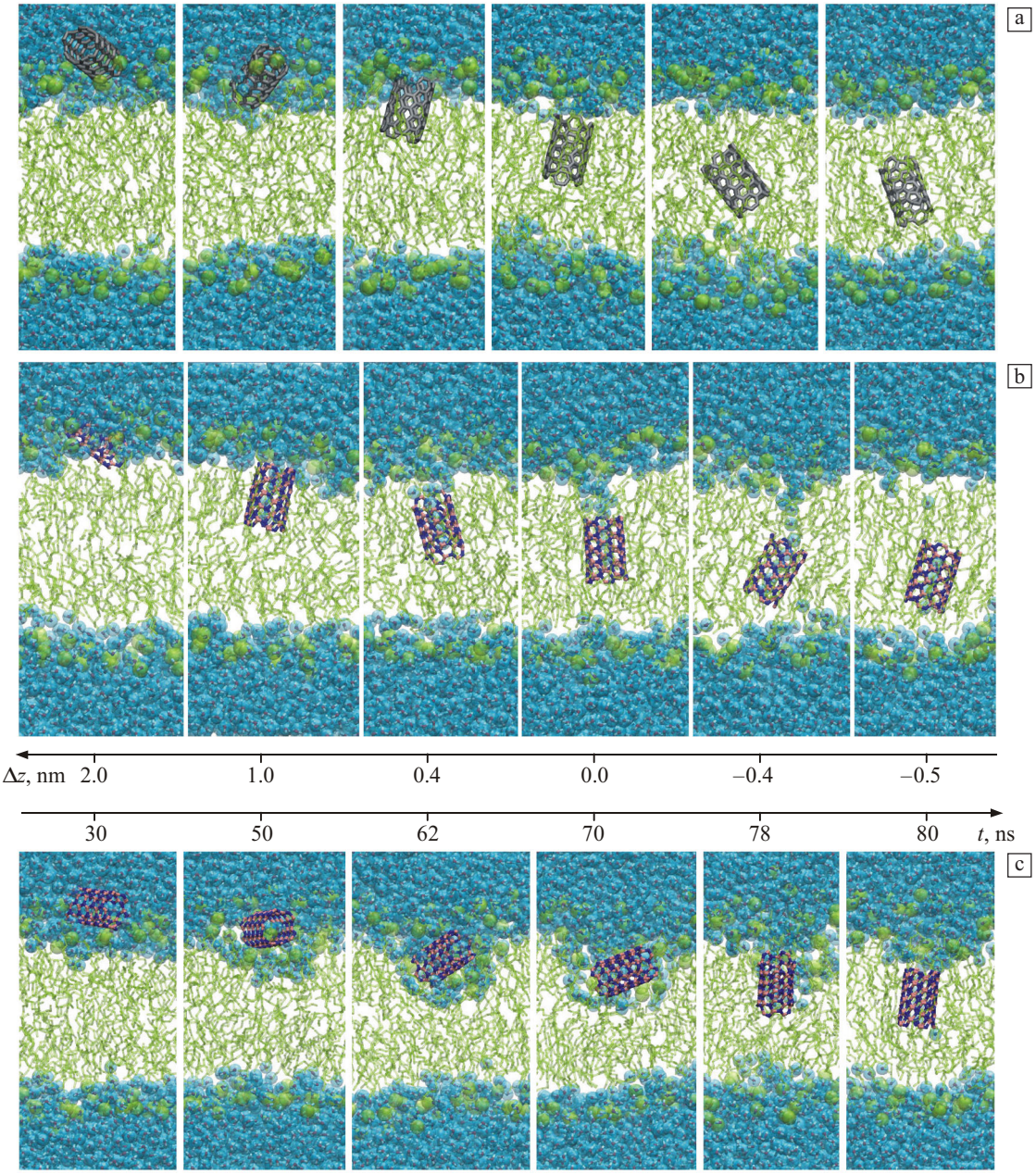

Fig. 2. Insertion of short (5, 5) nanotubes into a POPC lipid membrane during the pulling procedure of constant-velocity SMD simulation: (a) CNT, no water observed inside the CNT when it is in the lipophilic bilayer region, (b) BNNT (case ±0.4 *e*), BNNT brings 4–5 water molecules inside, (c) BNNT (case ±1.05 *e*), in this case BNNT behavior is hydrophilic, the hydrated shell around nanotube complicates the permeation into the lipophilic region of bilayer. Axes for time and Δ*z* are only for the snapshots in (b).

3. Boron nitride nanotubes: results and discussion

The partial atomic charges of BNNT are strongly environmentally dependent, as was demonstrated in [58] by using density functional theory (DFT). In particular, it was shown that partial charges on boron and nitrogen atoms may vary from ±0.37 *e* to ±1.05 *e* depending on both nanotube radius and the presence of water molecules inside the nanotube. In case of (5, 5) BNNT in vacuum, boron atoms had partial charges of 0.4 *e* and nitrogen atoms had partial charges of –0.4 *e*, whereas BNNT that contained 5–7 water molecules inside, have a strong electric dipoles with ±1.05 *e* [58]. In the present study we have tested two BNNT models with both sets of partial charges.

SMD simulations with constant velocity ($v = 0.05$ nm/ns) showed that BNNT (PAC set #1), unlike CNT, remain filled with 4–5 water molecules even in the hydrophobic core of the lipid bilayer (Figs. 2a and 2b). Moreover, during the penetration of BNNT into the membrane, a “water defect”

was observed, which had the form of a several-water-molecule long tail behind the penetrant until a depth $z = -0.4$ nm (Fig. 2b, $t = 78$ ns). The PMF profile has a local minimum -10 ± 5 kJ/mol at the membrane surface in the region of 2.4–2.6 nm from the bilayer center (Fig. 1, blue curve). The magnitude of the free energy barrier reached at 2.1–2.3 nm can be roughly estimated as 10.3 ± 8.6 kJ/mol, which is not far from the CNT case. Moving through the lipid head groups region, BNNT (both charge sets), like CNT, tend to be oriented parallel to the membrane surface, while, after the penetration into hydrophobic core of the bilayer, the nanotubes predominantly have "transmembrane" orientation and prefer to be parallel the lipid tails (Fig. 2). The CNT and BNNT (set #1) PMF profiles are fairly similar, the main difference being the depth of free energy well, which is 30% smaller for BNNT $\Delta F_{\mathrm{BNNT}} \approx -72$ kJ/mol (Fig. 1). The presence of this deep local free energy minimum inside the lipophilic bilayer region demonstrates the predominant hydrophobic behavior of the considered BNNT, which correlates with some experimental results of wetting tests conducted in air [59, 60]. However, since the penetrating single-walled BNNT, even with charges of ± 0.4 *e*, retain water molecules inside them during the translocation through the bilayer, we also have to look at the second case with partial charges ± 1.05 *e*.

The evaluated PMF profile for the BNNT model having PAC of ± 1.05 *e* differs substantially from the first BNNT case (Fig. 1). In this case the BN nanotube behaves as a hydrophilic nanoparticle and remains clothed in water shell during the penetration process up to a distance $z \approx 1$ nm from the center of the membrane (Fig. 2c). The formation of such a stable water shell strongly hampers the penetration of the nanotube into the hydrophobic core of the lipid bilayer. During the pulling process, the PMF is increasing and reaches values of up to 105 ± 21 kJ/mol at the membrane center (Fig. 1, red curve). This means that BNNT (set #2) is not stable inside the cell membrane and that penetration is not energetically favorable, i.e. in this case BN nanotubes do not spontaneously penetrate into and do not accumulate in the cell membrane. Therefore, BNNT with high partial charges would be less cytotoxic than the pristine and even functionalized CNTs. Moreover, BNNT (PAC set #2) has a quasi-stable configuration on the lipid-water interface, with PMF profile having a local minimum of -11 ± 3 kJ/mol at a distance of 2.4–2.6 nm from the membrane midplane.

The free energy estimations for the two BNNT models with their respective sets of PACs gave greatly differing results. However, it can be speculated that the free energy change for the real system may be in between the PMF profiles estimated for PAC set #1 and set #2. Additionally, in accordance with the study by Won and Aluru, the (5, 5) BNNT filled with water has the largest partial charges among zigzag BNNTs (*n*, *n*) with $n = 5, 6, 9, 10$ [58]. Based on this, it can be concluded that BNNTs with a larger diameter would demonstrate more hydrophobic behavior, and that zigzag (5, 5) BNNTs are at least less cytotoxic than (5, 5) CNT.

A more accurate choice of partial charges or/and their dependence on the environment will allow one to obtain more reliable results.

4. Methods

The modeled systems were constructed using VMD software [61] (http://www.ks.uiuc.edu/Research/vmd) and our own C/C++ functions library MoleSkola. Equilibration and SMD simulations were performed with the LAMMPS package (Sandia National Laboratory) [62, 63] (http://lammps.sandia.gov/index.html). The united atoms CHARMM36-UA force field [55] based on CHARMM36 FF [64] was used for lipids. The membrane was composed of 104 POPC lipids, having implicit hydrogens in acyl chains. Water was described with the TIP3P model [65]. The model of the carbon (5, 5) SWNT was made in accordance with Kaukonen et al. [56]. Lennard-Jones parameters for NT carbon atoms were $\sigma = 0.3534$ nm, $\varepsilon = 0.2929$ kJ/mol. Partial charges of NT carbon was zero. The CNT diameter and length were 0.68 nm and 1.11 nm, respectively. The modeled boron nitride SWNT was zigzag as well, having chirality (5, 5). The BNNT had a diameter of 0.69 nm and a length of 1.13 nm. The Lennard-Jones parameters for B atoms were $\sigma = 0.3453$ nm, $\varepsilon = 0.393$ kJ/mol, and for NT nitrogen $\sigma = 0.3365$ nm, $\varepsilon = 0.602$ kJ/mol, according to [38].

To describe BNNT electrostatics two different sets of PACs were used according to estimations obtained with DFT calculations by Won and Aluru [58]: PAC set #1: $Q_{\mathrm{B}} = 0.4$ *e*, $Q_{\mathrm{N}} = -0.4$ *e*; set #2: $Q_{\mathrm{B}} = 1.05$ *e*, $Q_{\mathrm{N}} = -1.05$ *e*. The first set corresponds to (5, 5) BNNT in vacuum, the second to BNNT filled with water molecules.

The equilibration of each system was conducted in NVT (constant volume and temperature) conditions with human body temperature 310 K during 4 ns with 1 fs integration step. All constant velocity SMD simulations were performed in NPT thermo-barostat conditions [66]. Employing of the United Atom POPC lipid model and the SHAKE algorithm [67] for the remaining hydrogen atoms, allowed us to use a time step of $\tau = 2$ fs. The entire system size was about 20 thousand atoms, with initial simulation box dimensions of $5.8 \times 5.8 \times 7.4$ nm. The pairwise interaction cutoff was 1.2 nm with 1.0 nm switching distance. Long-range electrostatics was computed using the PPPM algorithm [68] with a relative accuracy of 10^{-3}.

Free energy analysis was performed by potential of mean force (PMF) calculations [69] employing steered MD simulation with a constant velocity $v = 0.05$ nm/ns. In each simulation the initial position of the nanotube center of mass was $z = 3.5$ nm, where $z = 0$ corresponds to the membrane midplane. Total SMD simulation time was 290 ns for BNNT set #1, 220 ns for set #2 and 80 ns for CNT.

5. Conclusions

In this study, the free energy difference and barrier energy for the insertion of short boron nitride nanotubes into a cell membrane were calculated and compared with those for equivalently sized carbon nanotube. Two sets of partial atomic charges on boron and nitrogen atoms were considered, resulting in BNNTs with a slightly hydrophobic or hydrophilic behavior.

The potential of mean force analysis showed that BNNT with PAC of ±0.4 *e* has a 30% smaller depth of free energy well than the equivalently sized CNT. Moreover, CNT remained empty inside the lipid membrane whereas BNNT brings in several water molecules. The penetration BNNT with PAC of ±1.05 *e* into the cell membrane is energetically unfavorable, which indirectly indicates that in this case BNNT would have a smaller impact on the cell membrane and would be less cytotoxic than non-functionalized carbon nanotubes and nanoparticles.

It is important to note that the presented free energy values are still only rough estimation, due to the relatively high velocity of the pulling procedure we used, as well as the limited accuracy of the partial atomic charges and their assumed independence from the environment in the classical MD. For this reasons we regard our results as preliminary and recommend repeating the calculations using a lower velocity, or to perform sampling with long time accumulation.

The next logical step in modeling BNNT interaction with biological materials, in particular cell membranes, would be to incorporate some regularities of environment-induced charge alteration using, for example, simplified quantum mechanics approaches.

Acknowledgments

The authors thank Mikhail Popov (Berlin University of Technology, Germany) for useful discussions and help with the preparation of the publication. The present work was supported by the Russian Science Foundation (Grant No. 14-23-00096). All reported MD simulations were performed using cluster Lomonosov-1 of the Supercomputing Center (http://www.srcc.msu.su/nivc/index_engl.htm) of Lomonosov Moscow State University (MSU) [70].

References

1. Kroto HW, Heath JR, O'Brien SC, Curl RF, Smalley RE. C60: Buckminsterfullerene. Nature. 1985; 318: 162–163.
2. Iijima S. Helical microtubules of graphitic carbon. Nature. 1991; 354(6348): 56–58.
3. Anilkumar P, Lu F, Cao LG, Luo P, Liu JH, Sahu S, et al. Fullerenes for applications in biology and medicine. Current Medicinal Chem. 2011; 18(14): 2045–2059.
4. Chen Z, Ma L, Liu Y, Chen C. Applications of functionalized fullerenes in tumor theranostics. Theranostics. 2012; 2(3): 238–250.
5. Yang W, Thordarson P, Gooding JJ, Ringer SP, Braet F. Carbon nanotubes for biological and biomedical applications. Nanotechnology. 2007; 18(41): 412001.
6. Liu Z, Tabakman S, Welsher K, Dai H. Carbon nanotubes in biology and medicine: in vitro and in vivo detection, imaging and drug delivery. Nano Research. 2009; 2(2): 85–120.
7. Farmer VC, Fraser AR. Synthetic imogolite, a tubular hydroxy-aluminium silicate. Developments Sedimentology. 1979; 27: 547–553.
8. Farmer VC, Smith BFL, Tait JM. The stability, free energy and heat of formation of imogolite. Clay Miner. 1979; 14: 103–107.
9. Tenne R, Margulis L, Genut MEA, Hodes G. Polyhedral and cylindrical structures of tungsten disulphide. Nature. 1992; 360(6403): 444–446.
10. Remskar M, Mrzel A, Skraba Z, Jesih A, Ceh M, Demšar J, ..., Mihailovic D. Self-assembly of subnanometer-diameter single-wall MoS_2 nanotubes. Science. 2001; 292(5516): 479–481.
11. Enyashin AN, Ivanovskii AL. Calculating the atomic and electronic structure and magnetic properties of inorganic fullerenes. Russ J Phys Chem. 2005; 79(6): 940–945.
12. Rubio A, Corkill JL, Cohen ML. Theory of graphitic boron nitride nanotubes. Phys Rev B. 1994; 49(7): 5081.
13. Chopra NG, Luyken RJ, Cherrey K, Crespi VH, Cohen ML, Louie SG, Zettl A. Boron nitride nanotubes. Science. 1995; 269(5226): 966–967.
14. Badzian AR, Appenheimer S, Niemyski T, Olkusnik E. In: Glaski FA, editor. Third international conference on CVD, Salt Lake City, UT, 1972. Hindsdale, IL: Am. Nuclear Soc.; 1972.
15. Miyamoto Y, Rubio A, Cohen ML, Louie SG. Chiral tubules of hexagonal BC 2 N. Phys Rev B. 1994; 50(7): 4976.
16. Miyamoto Y, Rubio A, Louie SG, Cohen ML. Electronic properties of tubule forms of hexagonal BC 3. Phys Rev B. 1994; 50(24): 18360.
17. Xia X, Jelski DA, Bowser JR, George TF. MNDO study of boron-nitrogen analogs of buckminsterfullerene. J Am Chem Soc. 1992; 114(16): 6493–6496.
18. Pokropivny VV, Skorokhod VV, Oleinik GS, Kurdyumov AV, Bartnitskaya TS, Pokropivny AV, ..., Sheichenko DM. Boron nitride analogs of fullerenes (the fulborenes), nanotubes, and fullerites (the fulborenites). J Solid State Chem. 2000; 154(1): 214–222.
19. Sheichenko DM, Pokropivny AV, Pokropivny VV. Quantum-chemistry calculation of $B \sim nN \sim n$-rings (n = 1–6) and fulborenes, the fullerene-like molecules $B \sim nN \sim n$ (n = 12, 24, 60). Semiconductor Physics Quantum Electronics Optoelectronics. 2000; 3(4): 545–549.
20. Linnolahti M, Pakkanen TA. Molecular structures of alumina nanoballs and nanotubes: A theoretical study. Inorg Chem. 2004; 43(3): 1184–1189.
21. Lee K, Mazare A, Schmuki P. One-dimensional titanium dioxide nanomaterials: nanotubes. Chem Rev. 2014; 114(19): 9385–9454, and references therein.
22. Levi R, Bar-Sadan M, Albu-Yaron A, Popovitz-Biro R, Houben L, Shahar C, Enyashin A, Seifert G, Prior Y, Tenne R. Hollow V2O5 nanoparticles (fullerene-like analogues) prepared by laser ablation. J Am Chem Soc. 2010; 132(32): 11214.

23. Fagan SB, Baierle RJ, Mota R, da Silva AJ, Fazzio A. *Ab initio* calculations for a hypothetical material: Silicon nanotubes. Phys Rev B. 2000; 61(15): 9994.
24. Pokropivny VV. Non-carbon nanotubes (Review). Part 1. Synthesis methods. Powder Metallurgy Metal Ceramics. 2001; 40(9-10): 485–496.
25. Pokropivny VV. Non-carbon nanotubes (Review). Part 2. Types and structure. Powder Metallurgy Metal Ceramics. 2001; 40(11-12): 582–594.
26. Pokropivny VV. Non-carbon nanotubes (Review). Part 3. Properties and applications. Powder Metallurgy Metal Ceramics. 2002; 41(3-4): 123–135.
27. Genchi GG, Ciofani G. Bioapplications of boron nitride nanotubes. Nanomedicine. 2015; 10(22): 3315–3319.
28. Mele EJ, Král P. Electric polarization of heteropolar nanotubes as a geometric phase. Phys Rev Lett. 2002; 88(5): 056803.
29. Ciofani G, Danti S, D'Alessandro D et al. Enhancement of neurite outgrowth in neuronal-like cells following boron nitride nanotube-mediated stimulation. ACS Nano. 2010; 4: 6267–6277.
30. Lan HP, Ye LH, Zhang S, Peng LM. Transverse dielectric properties of boron nitride nanotubes by *ab initio* electric field calculations. Appl Phys Lett. 2009; 94(18): 183110.
31. Chen X, Wu P, Rousseas M et al. Boron nitride nanotubes are noncytotoxic and can be functionalized for interaction with proteins and cells. J Am Chem Soc. 2009; 131: 890–891.
32. Ferreira TH, Hollanda LM, Lancellotti M, de Sousa EMB. Boron nitride nanotubes chemically functionalized with glycol chitosan for gene transfection in eukaryotic cell lines. J Biomed Mater Res A. 2015; 103: 2176–2185.
33. Weng Q, Wang B, Wang X, Hanagata N, Li X, Liu D, Wang X, Jiang X, Bando Y, Golberg D. Highly water-soluble, porous, and biocompatible boron nitrides for anticancer drug delivery. ACS Nano. 2014; 8(6): 6123–6130.
34. Danti S, Ciofani G, Moscato S et al. Boron nitride nanotubes and primary human osteoblasts: in vitro compatibility and biological interactions under low frequency ultrasound stimulation. Nanotechnology. 2013; 24: 465102.
35. Nakamura H, Koganei H, Miyoshi T, Sakurai T, Ono K, Suzuki M. Antitumor effect of boron nitride nanotubes in combination with thermal neutron irradiation on BNCT. Bioorg Med Chem Lett. 2015; 25: 172–174.
36. Lahiri D, Singh V, Benaduce AP, Seal S, Kos L, Agarwal A. Boron nitride nanotube reinforced hydroxyapatite composite: mechanical and tribological performance and in-vitro biocompatibility to osteoblasts. J Mech Behav Biomed Mat. 2011; 4: 44–56.
37. Zhi CY, Bando Y, Tang CC, Honda S, Kuwahara H, Golberg D. Boron nitride nanotubes/polystyrene composites. J Mater Res. 2006; 21(11): 2794–2800.
38. Azamat J, Sardroodi JJ. The permeation of potassium and chloride ions through nanotubes: a molecular simulation study. Monatshefte Chemie-Chemical Monthly. 2014; 145(6): 881–890.
39. Zhi C, Bando Y, Tang C, Golberg D. Boron nitride nanotubes. Mater Sci Eng R Rep. 2010; 70(3): 92–111.
40. Thomas M, Enciso M, Hilder TA. Insertion mechanism and stability of boron nitride nanotubes in lipid bilayers. J Phys Chem B. 2015; 119(15): 4929–4936.
41. Baoukina S, Monticelli L, Tieleman DP. Interaction of pristine and functionalized carbon nanotubes with lipid membranes. J Phys Chem B. 2013; 117(40): 12113–12123.
42. Marrink SJ, De Vries AH, Mark AE. Coarse grained model for semiquantitative lipid simulations. J Phys Chem B. 2004; 108(2): 750–760.
43. Marrink SJ, Risselada HJ, Yefimov S, Tieleman DP, de Vries AH. The MARTINI force field: coarse grained model for biomolecular simulations. J Phys Chem B. 2007; 111(27): 7812–7824.
44. Monticelli L. On atomistic and coarse-grained models for C60 fullerene. J Chem Theor Comp. 2012; 8(4): 1370–1378.
45. Kraszewski S, Bianco A, Tarek M, Ramseyer C. Insertion of short amino-functionalized single-walled carbon nanotubes into phospholipid bilayer occurs by passive diffusion. PLoS One. 2012; 7(7): e40703.
46. Höfinger S, Melle-Franco M, Gallo T, Cantelli A, Calvaresi M, Gomes JA, Zerbetto F. A computational analysis of the insertion of carbon nanotubes into cellular membranes. Biomater. 2011; 32(29): 7079–7085.
47. Kar P, Seel M, Weidemann T, Höfinger S. Theoretical mimicry of biomembranes. FEBS Lett. 2009; 583(12): 1909–1915.
48. Gangupomu VK, Capaldi FM. Interactions of carbon nanotube with lipid bilayer membranes. J Nanomater. 2011; 2011: 830436.
49. Pogodin S, Baulin VA. Can a carbon nanotube pierce through a phospholipid bilayer? ACS Nano. 2009; 4(9): 5293–5300.
50. Pogodin S, Baulin VA. Coarse-grained models of phospholipid membranes within the single chain mean field theory. Soft Matter. 2010; 6: 2216–2226.
51. Bedrov D, Smith GD, Davande H, Li L. Passive transport of C60 fullerenes through a lipid membrane: a molecular dynamics simulation study. J Phys Chem B. 2008; 112(7): 2078–2084.
52. Bedrov D, Smith GD, Li L. Molecular dynamics simulation study of the role of evenly spaced poly (ethylene oxide) tethers on the aggregation of C60 fullerenes in water. Langmuir. 2005; 21(12): 5251–5255.
53. Rodriguez-Gomez D, Darve E, Pohorille A. Assessing the efficiency of free energy calculation methods. J Chem Phys. 2004; 120: 3563–3578.
54. Darve E, Rodriguez-Gomez D, Pohorille A. Adaptive biasing force method for scalar and vector free energy calculations. J Chem Phys. 2008; 128: 144120–144113.
55. Lee S, Tran A, Allsopp M, Lim JB, Hénin J, Klauda JB. CHARMM36 united atom chain model for lipids and surfactants. J Phys Chem B. 2014; 118(2): 547–556.
56. Kaukonen M, Gulans A, Havu P, Kauppinen E. Lennard-Jones parameters for small diameter carbon nanotubes and water for molecular mechanics simulations from van der Waals density functional calculations. J Comp Chem. 2012; 33(6): 652–658.
57. Torrie GM, Valleau JP. Nonphysical sampling distributions in Monte Carlo free-energy estimation: Umbrella sampling. J Comp Phys. 1977; 23(2): 187–199.
58. Won CY, Aluru NR. Structure and dynamics of water confined in a boron nitride nanotube. J Phys Chem C. 2008; 112(6): 1812–1818.
59. Lee CH, Drelich J, Yap YK. Superhydrophobicity of boron nitride nanotubes grown on silicon substrates. Langmuir. 2009; 25(9): 4853–4860.

60. Yum K, Yu MF. Measurement of wetting properties of individual boron nitride nanotubes with the Wilhelmy method using a nanotube-based force sensor. Nano Lett. 2006; 6(2): 329–333.
61. Humphrey W, Dalke A, Schulten K. VMD: visual molecular dynamics. J Mol Graphics. 1996; 14(1): 33–38.
62. Plimpton S. Fast parallel algorithms for short-range molecular dynamics. J Comp Phys. 1995; 117(1): 1–19.
63. Plimpton S, Crozier P, Thompson A. LAMMPS-large-scale atomic/molecular massively parallel simulator. Sandia Natl Lab. 2007; 18.
64. MacKerell AD, Bashford D, Bellott MLDR, Dunbrack RL, Evanseck JD, Field MJ, et al. All-atom empirical potential for molecular modeling and dynamics studies of proteins. J Phys Chem B. 1998; 102(18): 3586–3616.
65. Jorgensen WL, Chandrasekhar J, Madura JD, Impey RW, Klein ML. Comparison of simple potential functions for simulating liquid water. J Chem Phys. 1983; 79(2): 926–935.
66. Parrinello M, Rahman A. Polymorphic transitions in single crystals: A new molecular dynamics method. J Appl Phys. 1981; 52(12): 7182–7190.
67. Ryckaert JP, Ciccotti G, Berendsen HJ. Numerical integration of the cartesian equations of motion of a system with constraints: molecular dynamics of n-alkanes. J Comp Phys. 1977; 23(3): 327–341.
68. Hockney RW, Eastwood JW. Computer simulation using particles. Adam Hilger: New York; 1989.
69. Izrailev S, Stepaniants S, Isralewitz B, Kosztin D, Lu H, Molnar F, Wriggers W, Schulten K. Steered molecular dynamics. In: Deuflhard P, Hermans J, Leimkuhler B, Mark AE, Reich S, Skeel RD, editors. Computational molecular dynamics: challenges, methods, ideas. Vol. 4 of lecture notes in computational science and engineering. Berlin: Springer-Verlag; 1998.
70. Sadovnichy V, Tikhonravov A, Voevodin Vl, Opanasenko V. "Lomonosov": Supercomputing at Moscow State University. In: Contemporary high performance computing: From petascale toward exascale (Chapman & Hall/CRC Computational Science). Boca Raton, USA: CRC Press; 2013.